J Ther Eng, Vol. 10, No. 5, pp. 1107−1119, September, 2024

Journal of Thermal Engineering
Web page info: https://jten.yildiz.edu.tr
DOI: 10.14744/thermal.0000854

Research Article

Influence of buoyancy forces in MHD non-Newtonian convective nanofluid utilizing Buongiorno's Model induced by 3D exponential sheet

Saloni GUPTA[1,*], Parmod Kumar SHARMA[2], Sanjay KUMAR[2], Chinta Mani TIWARI[1]

[1]*Maharishi School of Science, Maharishi School of Information Technology, Lucknow, 226013, India*
[2]*Department of Applied Sciences, KIET Group of Institutions, Ghaziabad, 201206, India*

ARTICLE INFO

Article history
Received: 17 October 2023
Revised: 04 May 2024
Accepted: 04 June 2024

Keywords:
Buongiorno's Model; Buoyancy forces; Casson Fluid; Chemical Reaction; Nanofluid; Shooting Method

ABSTRACT

The designation of this research is to scrutinize the influence of convective nanofluids over a three-dimensional exponential surface with chemical reactive species in a free stream fluid flow by following Buongiorno's model. The continuity, momentum, energy, concentration and motile microorganism density partial differential equations that make up the physical governing equation problems are simultaneously transformed into ordinary differential equations system. By using MATLAB programming, the RKF approach has been followed in order to implement the shooting technique to solve this system that explores how changing fluid parameters affect the profile of physical quantities of interest. A parametric analysis has been done in the current study. The effects of fluid parameters such as chemical reaction, Brownian motion, free stream velocity, Lewis number, thermophoresis, and Prandtl number on concentration, temperature, and velocity profiles are graphically represented. Moreover, Contour plots are also drawn against computational fluid parameters to get desired results. Furthermore, calculated results are correlated with already existing outcomes along with residual error. It is inferred that; thermal and concentration fields increase for higher thermal and concentration Biot numbers serially. Additionally, it is found that skin friction coefficient declines with inclination in thermophoresis Nt ($1.0 \leq Nt \leq 3.0$) and Prandtl number Pr ($1.0 \leq Pr \leq 4.0$). The present investigation aims to support production businesses in achieving the desired level of quality of their products by effectively managing the transport phenomena.

Cite this article as: Gupta S, Sharma PK, Kumar S, Tiwari CM. Influence of buoyancy forces in MHD non-Newtonian convective nanofluid utilizing Buongiorno's Model induced by 3D exponential sheet. J Ther Eng 2024;10(5):1107−1119.

INTRODUCTION

Stream conduct over extending surfaces has drawn attention of many researchers because of its wide space of modern and fabricating applications like fake strands, petrol ventures, metal turning, polymer handling and so forth. Crane [1] concentrated on the stream towards an extending sheet. Sarma and Rao [2] explored the stream conduct in viscoelastic liquid over an extending sheet. Additionally, Radiation impact with hotness source was considered by

***Corresponding author.**
*E-mail address: saloni.20.jindal@gmail.com

This paper was recommended for publication in revised form by Editor-in-Chief Ahmet Selim Dalkılıç

Manjunatha et al. [3] over permeable medium. In ongoing many years, heat move angles are substantially more significant for issues identified with extending sheet because of its warming and cooling essential variables for making superior grade of eventual outcome. Fourier [4] proposed law of heat conduction very first and revealed that this law gives premise to discover the hotness move conduct under various conditions. Yet, this model has significant disadvantage that it offers numerical expression of energy in illustrative structure. From that point onward, Cattaneo [5] has acquired new statures of Fourier's law with warm unwinding time because of the conditions that are in illustrative structure which moved into exaggerated structure. Very recently, heat dissipation impact under different physical conditions has been analyzed by researchers [6-9].

Researchers are paying more attention to nanofluid because of its physical properties and uses in many areas, mainly production, industry, and medicine. These tiny fluids have lots of important properties for research, like low resistivity and unique thermophysical aspects. In the last few decades, the word "nanofluid" has been a topic of interest in a number of scientific groups because it is able to transfer heat quickly. Choi and Eastman [10] identified a brand-new class of fluids called nanofluids. Because they have a high rate of heat transmission, nanofluids are of interest to many scientists and academics. Compared to solids, fluids are less effective in transferring heat. The creation of ultrafine particles enhances the thermal conductivity of nanofluids, according to Xuan and Li [11]. Through Brownian motion and thermophoresis diffusion, Buongiorno [12] created a methodical strategy that boosted the heat exchange phenomenon. Moreover, influence of activation energy over porous surface in presence of Carreau nanofluid has been presented by Shahid et al. [13]. Din et al. [14] studied the significance of bio-convection and slip conditions over wedge by utilizing tangential hyperbolic and Carreau nanofluids. Three-dimensional second-class nanofluid flow across a stretched surface has been studied by Ahmad et al. [15] using the Optimal Homotopy Analysis approach. The investigation of non-Newtonian fluids has numerous real-world uses in technology and other fields of study. Non-Newtonian fluid mechanics has a lot of interesting and important uses in the fields of engineering, healthcare, and the applied sciences. Since both the surrounding air and the ocean are fluids, the studies of fluids are essential to metrology, oceanography, and hydrology. Identifying the flow of various biological fluids is important for successful medical treatment. When hybrid nanoliquids were subjected to nonlinear solar radiation, Acharya et al. [16] investigated how various solar thermal devices affected the flow fluctuations and heat exchange properties of the materials. Very recently, Rana et al. [17] uses ANN to predict the stable solutions and critical points in viscoelastic fluids induced by horizontal sheet. In recent years, nanofluid flow in presence of Magnetohydrodynamics under different physical aspects has been explored by authors [18-21].

The field of MHD has important applications in the medical and industrial sciences. MHD has a wide range of potential uses, including endoscopy, cell separation, cancer tumor treatment, drug targeting and surgical blood flow control. MHD utilized in medication i.e., growth or disease treatment. A stagnation point MHD nanofluid stream was mathematically examined by Anwar et al. [22] induced by stretching surface. Then Shawky et al. [23] discussed Williamson nanofluid towards an extending plot. Vajravelu and Cannon [24] inspected the stream conduct of liquid on non-direct extending sheet. Additionally, a blended MHD nanofluid stream alongside entropy and convective investigation on a non-straight extending sheet was addressed by Matin et al. [25]. Jain and Choudhary [26] examined the Soret and Dufour impacts with MHD stream utilizing compound responses. Siddheshwar and Mahabaleshwar [27] concentrated on the issue of hotness and stream transportation on non-straight extending sheet with pull/infusion. By using hybrid nanofluids flow in presence of Stefan blowing bio-convection has been analyzed by Rana et al. [28]. The opinions of a few different specialists [29-36], considered a different aspect of those kinds of problems under diverse circumstances.

Motivated by the already existing literature uncovers that no such study has been made to the till now. Current research focuses on the effect of transport phenomenon by creating outcome of MHD nanofluid flow and free stream in presence of compound response towards an extending surface. The philosophy embraced addresses whole framework through Runge Kutta Fehlberg strategy by following shooting procedure utilizing ODE45 solver. The numerical troubles showing up in the nanofluid conditions drove us to utilize the mathematical methodology. Utilizing the concept of buoyancy forces and nanoparticles, current research is relevant to novel microbial fuel cell technologies in exponential surface. The current research's results assist the biological, technological, and manufacturing domains in producing desired products that make this study to novel one.

MATERIALS AND METHODS

3D non-Newtonian nanofluid model with magnetohydrodynamic flow induced by stretching surface is considered in the current research (Figure 1). In this model, thermophoresis and Brownian motion impact of nanofluid has been incorporated among stretched velocities $U_w = U_0 \exp\left(\frac{x+y}{L}\right)$, $V_w = V_0 \exp\left(\frac{x+y}{L}\right)$ in x and y direction serially. Buoyancy forces along with free stream velocity are incorporated in the current study. Modeled equations are shown as ([14], [37-39]):

$$\frac{\partial u}{\partial x} + \frac{\partial v}{\partial y} + \frac{\partial w}{\partial z} = 0 \tag{1}$$

$$u\frac{\partial u}{\partial x}+v\frac{\partial u}{\partial y}+w\frac{\partial u}{\partial z}=\nu\left(1+\frac{1}{\beta}\right)\frac{\partial^2 u}{\partial z^2}+g\beta_C\left(C-C_\infty\right)+g\beta_T\left(T-T_\infty\right)$$
$$-\frac{\sigma B_0^2}{\rho}u+U_\infty\frac{\sigma B_0^2}{\rho}+U_\infty\frac{\partial U_\infty}{\partial z} \quad (2)$$

$$u\frac{\partial v}{\partial x}+v\frac{\partial v}{\partial y}+w\frac{\partial v}{\partial z}=\nu\left(1+\frac{1}{\beta}\right)\frac{\partial^2 v}{\partial z^2}+g\beta_C\left(C-C_\infty\right)+g\beta_T\left(T-T_\infty\right)$$
$$-\frac{\sigma B_0^2}{\rho}v+U_\infty\frac{\sigma B_0^2}{\rho}+U_\infty\frac{\partial U_\infty}{\partial z} \quad (3)$$

$$u\frac{\partial T}{\partial x}+v\frac{\partial T}{\partial y}+w\frac{\partial T}{\partial z}=\frac{k}{(\rho C_p)_{nf}}\frac{\partial^2 T}{\partial z^2}+\frac{(\rho C_p)_p}{(\rho C_p)_{nf}}\left[D_B\frac{\partial T}{\partial z}\frac{\partial C}{\partial z}+\frac{D_T}{T_\infty}\left(\frac{\partial T}{\partial z}\right)^2\right] \quad (4)$$

$$u\frac{\partial C}{\partial x}+v\frac{\partial C}{\partial y}+w\frac{\partial C}{\partial z}=D_B\frac{\partial^2 C}{\partial z^2}+\frac{D_T}{T_\infty}\frac{\partial^2 T}{\partial z^2}-K_r(C-C_\infty), \quad (5)$$

Using similarity variables:

$$v=U_0\exp\left(\frac{x+y}{L}\right)g'(\xi),\quad u=U_o\exp\left(\frac{x+y}{L}\right)f'(\xi),$$
$$\xi=\sqrt{\frac{U_0}{2\nu L}}\exp\left(\frac{x+y}{L}\right)z$$
$$w=-\sqrt{\frac{\nu U_o}{2L}}\exp\left(\frac{x+y}{L}\right)\left[f(\xi)+\xi f'(\xi)+g(\xi)+\xi g'(\xi)\right], \quad (6)$$
$$\Theta(\xi)=\frac{T-T_\infty}{T_w-T_\infty}\quad\text{and}\quad\Phi=\frac{C-C_\infty}{C_w-C_\infty}$$

Considered boundary conditions:

$$u=U_w=U_0\exp\left(\frac{x+y}{L}\right),\ v=V_w=V_0\exp\left(\frac{x+y}{L}\right)\ \text{at}\ w=0$$
$$-k\left(\frac{\partial T}{\partial z}\right)=h_f\left(T_w-T\right),\ -D_B\left(\frac{\partial C}{\partial z}\right)=h_s\left(C_w-C\right)\ \text{at}\ z=0 \quad (7)$$
$$u\to a\exp\left(\frac{x+y}{L}\right),\ v\to 0,\ T\to T_\infty,\ C\to C_\infty\ \text{as}\ z\to\infty$$

Transformed governing equations are:

$$\left(1+\frac{1}{\beta}\right)f'''+\left(f+g\right)f''-2\left(f'+g'\right)f'+2\left(L_1\theta+L_2\phi\right)-M(f'-\lambda)+\lambda^2=0 \quad (8)$$

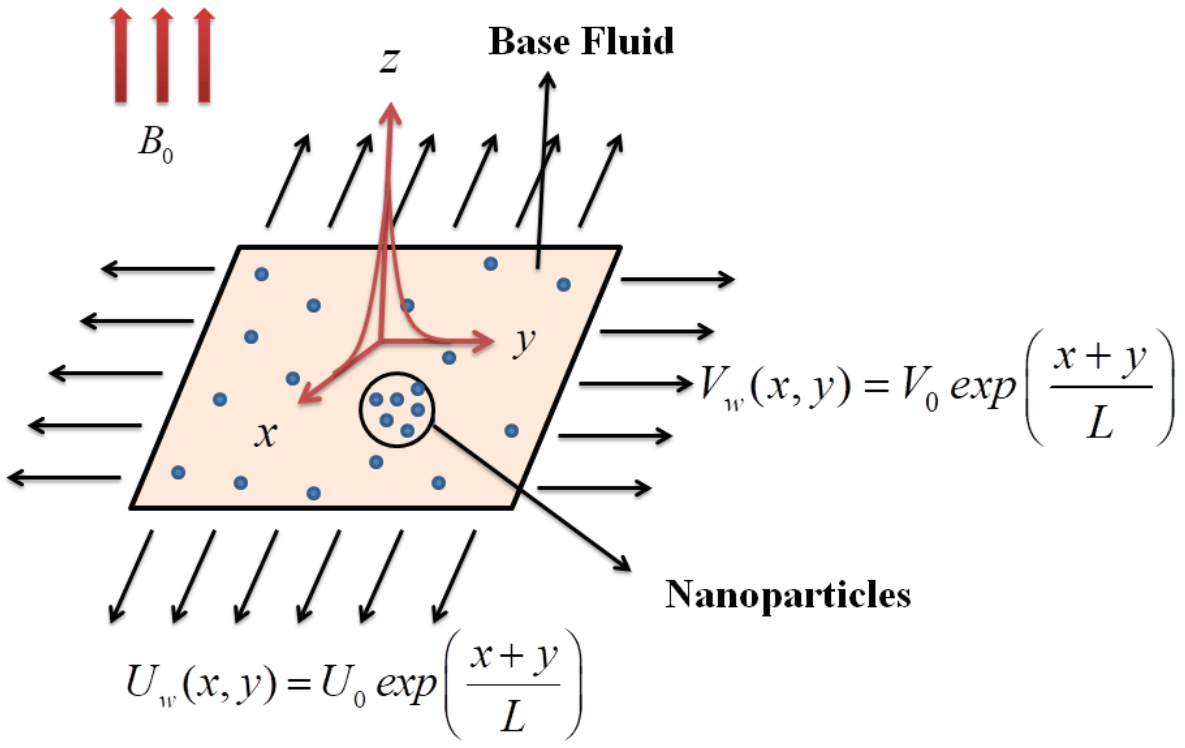

Figure 1. Physical Model of the problem.

$$\left(1+\frac{1}{\beta}\right)g'''+(f+g)g''-2(f'+g')g'+2(L_1\theta+L_2\phi)-M(g'-\lambda)+\lambda^2=0 \quad (9)$$

$$\theta''+Pr\left[(f+g)\theta'+Nb\,\theta'\phi'+Nt\,\theta'^2\right]=0 \quad (10)$$

$$\phi''+Le\,Pr(f+g)\phi'+\left(\frac{Nt}{Nb}\right)\theta''-Le\,Pr\,Cr\,\phi=0 \quad (11)$$

Reduced B.C's are:

$$\begin{aligned} &f'=1,\ \ g'=1,\ \ \theta'(0)=-e\left[1-\theta(0)\right],\ \ \phi'(0)=-h\left[1-\phi(0)\right]\\ &f'\to\lambda,\ \ g'\to 0,\ \ \theta\to 0,\ \ \phi\to 0 \end{aligned} \quad (12)$$

Cf_x, Cf_y, Nu_x and Sh_x are defined as:

$$\begin{aligned} &Cf_x=\frac{\tau_{xz}}{\rho U_w^{\,2}},\ Cf_y=\frac{\tau_{yz}}{\rho U_w^{\,2}},\ Nu_x=\frac{-x}{(T_w-T_\infty)}\left(\frac{\partial T}{\partial z}\right)\Bigg|_{z=0}\\ &\text{and}\ \ Sh_x=\frac{-x}{(C_w-C_\infty)}\left(\frac{\partial C}{\partial z}\right)\Bigg|_{z=0} \end{aligned} \quad (13)$$

Physical quantities of interest are:

$$\begin{aligned} &Cf_x\,\mathrm{Re}_x^{1/2}=\left(1+\frac{1}{\beta}\right)f''(0),\ \ Cf_y\,\mathrm{Re}_x^{1/2}=\left(1+\frac{1}{\beta}\right)g''(0),\\ &Nu_x\,\mathrm{Re}_x^{-1/2}=-\theta'(0),\ \ Sh_x\,\mathrm{Re}_x^{-1/2}=-\phi'(0) \end{aligned} \quad (14)$$

Where Re_x shows Reynolds's number.

Numerical Solution

The system of D.E's (8)-(11) and B.C's (12) has been solved with Runge-Kutta-Fehlberg approach by following shooting procedure, as indicated in a flowchart in Figure 2. To get a numerical solution, the step size is set to 0.01 and the maximum value to 10. Main advantage of this technique is that it has 5th order truncation error over other numerical techniques. Additionally, as compared to other numerical techniques, the computation of the solution is simpler and easier. The well-known programme MATLAB is used in the current analysis to do computations utilizing the ODE45 solver. 1st order D.E's have been created from the coupled D.E's (8)-(11) in this case. The controlling nonlinear O.D.E's are reconfigured as follows for this purpose:

$$f'''=-\frac{1}{\left(1+\frac{1}{\beta}\right)}\left[(f+g)f''-2(f'+g')f'+2(L_1\theta+L_2\phi)-M(f'-\lambda)+\lambda^2\right] \quad (15)$$

$$g'''=-\frac{1}{\left(1+\frac{1}{\beta}\right)}\left[(f+g)g''-2(f'+g')g'+2(L_1\theta+L_2\phi)-M(g'-\lambda)+\lambda^2\right] \quad (16)$$

$$\theta''=-Pr\left[(f+g)\theta'+Nb\,\theta'\phi'+Nt\,\theta'^2\right] \quad (17)$$

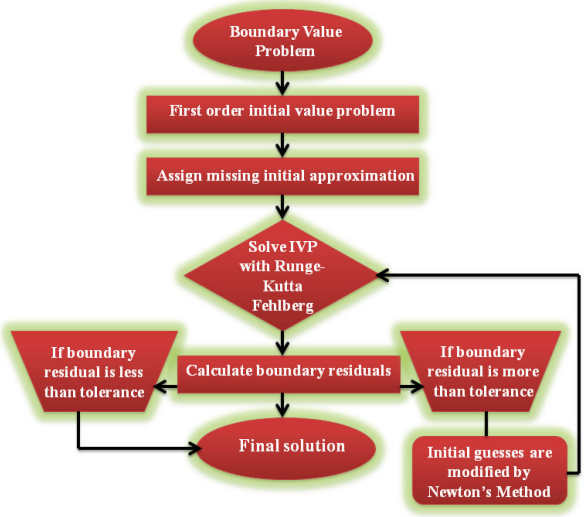

Figure 2. Flow chart of shooting technique.

$$\begin{aligned} \phi''=&-Le\,Pr(f+g)\phi'+Pr\left(\frac{Nt}{Nb}\right)\left[(f+g)\theta'+Nb\,\theta'\phi'+Nt\,\theta'^2\right]\\ &+Le\,Pr\,Cr\,\phi \end{aligned} \quad (18)$$

Now, a defined new set of variables is provided below to convert the equations previously defined into the first-order O.D.E's:

$$\begin{aligned} &f=\tilde{k}(1),f'=\tilde{k}(2),f''=\tilde{k}(3),f'''=\tilde{k}(3)'\\ &g=\tilde{k}(4),g'=\tilde{k}(5),g''=\tilde{k}(6),g'''=\tilde{k}(6)'\\ &\theta=\tilde{k}(7),\theta'=\tilde{k}(8),\theta''=\tilde{k}(8)'\\ &\phi=\tilde{k}(9),\phi'=\tilde{k}(10),\phi''=\tilde{k}(10)' \end{aligned} \quad (19)$$

Equations (15)-(18) are changed into the following system of D.E's by using Equation (19) to them:

$$\tilde{k}(1)'=\tilde{k}(2) \quad (20)$$

$$\tilde{k}(2)'=\tilde{k}(3) \quad (21)$$

$$\begin{aligned} \tilde{k}(3)'=&-\frac{\beta}{(1+\beta)}\left[\left\{\tilde{k}(1)+\tilde{k}(4)\right\}\tilde{k}(3)-2\left\{\tilde{k}(2)+\tilde{k}(5)\right\}\tilde{k}(2)\right.\\ &\left.+2\left\{L_1\tilde{k}(7)+L_2\tilde{k}(9)\right\}-M\left\{\tilde{k}(2)-\lambda\right\}+\lambda^2\right] \end{aligned} \quad (22)$$

$$\tilde{k}(4)'=\tilde{k}(5) \quad (23)$$

$$\tilde{k}(5)'=\tilde{k}(6) \quad (24)$$

$$\begin{aligned} \tilde{k}(6)'=&-\frac{\beta}{(1+\beta)}\left[\left\{\tilde{k}(1)+\tilde{k}(4)\right\}\tilde{k}(6)-2\left\{\tilde{k}(2)+\tilde{k}(5)\right\}\tilde{k}(5)\right.\\ &\left.+2\left\{L_1\tilde{k}(7)+L_2\tilde{k}(9)\right\}-M\left\{\tilde{k}(5)-\lambda\right\}+\lambda^2\right] \end{aligned} \quad (25)$$

$$\tilde{k}(7)' = \tilde{k}(8) \quad (26)$$

$$\tilde{k}(8)' = -Pr\left[\left\{\tilde{k}(1)+\tilde{k}(4)\right\}\tilde{k}(8) + Nb\,\tilde{k}(8)\,\tilde{k}(10) + Nt\,\tilde{k}(8)^2\right] \quad (27)$$

$$\tilde{k}(9)' = \tilde{k}(10) \quad (28)$$

$$\tilde{k}(10)' = -Le\,Pr\left\{\tilde{k}(1)+\tilde{k}(4)\right\}\tilde{k}(10) - \left(\frac{Nt}{Nb}\right)\tilde{k}(8)' + Le\,Pr\,Cr\,\tilde{k}(9) \quad (29)$$

RESULTS AND DISCUSSION

For adjusting fluid parameter *Pr* in the absence of magnetohydrodynamic flow, the estimated findings for Nusselt number are compared with those from Abolbashari et al. [40] and Khan and Pop [41] in the current analysis (Table 1). When compared to the conclusions of the current literature, it is found that the results are very accurate. The results ($f''(0)$, $g''(0)$), $-\theta'(0)$, $-\phi'(0)$, respectively, for fixed values of governing fluid parameters as e = 0.1; thermal Biot number, h = 0.1; concentration Biot number, λ = 0.1; free stream velocity parameter, $L1$ = 0.3; thermal buoyancy parameter, $L2$ = 0.3; solutal buoyancy parameter, M = 0.1; magnetic parameter, c = 0.1; stretching ratio parameter, β = 0.1; Casson Fluid parameter, Pr = 0.72; Prandtl number, Nb = 2.5; Brownian motion, Nt = 0.5; thermophoresis, Le = 2; Lewis number, Cr = 0.5; chemical reaction parameter are shown in Table 2-4.

Influence of free stream velocity λ over velocity profile $f'(\xi)$ has been presented in Figure 3(a) and it shows that velocity profile enhances with enhancement in free stream velocity ranging from $0.00 \le \lambda \le 0.20$. Figure 3(b) shows variety in liquid speed against attractive boundary M. Presence of attractive boundary M opposes the liquid molecule to move uninhibitedly and fundamental purpose for the obstruction is that attractive boundary M produces Lorentz power and this attraction conduct can be taken on for controlling the smooth motion. Accordingly, improvement in the worth of attractive boundary M causes the declination of speed dissemination. Figure 4(a) inspects temperature appropriation variety against the liquid boundary Brownian movement boundary Nb. Liquid temperature upgrades for higher Nb and in result neighborhood Nusselt number declines. Figure 4(b) ponders the effect of liquid temperature under the result of Nt. Temperature slope tumbles down for higher upsides of

Table 1. Comparison of Nusselt number along with residual error against Prandtl number

Pr	Abolbashari et al. [40]	Residual error	Khan and Pop [41]	Residual error	Present result
0.7	0.4539	-0.00055	0.4539	-0.00055	0.45445
7.0	1.8954	0.00000	1.8954	0.00000	1.89540
70	-	-	6.4621	-0.00009	6.46219

Table 2. Values of $f''(0)$ and $g''(0)$ for variables β, λ and M

β	λ	M	$f''(0)$	$g''(0)$
0.01	0.1	0.1	-0.187812892074880	-0.197270167668150
0.02	-	-	-0.254551983960999	-0.263917474359195
0.03	-	-	-0.307454811452548	-0.316858676272375
0.04	-	-	-0.352129703749639	-0.361620638351058
0.05	-	-	-0.391204404750134	-0.400800776174053
0.1	0.00	-	-0.550714648307227	-0.550714648307190
-	0.05	-	-0.545294633456807	-0.550592350184165
-	0.10	-	-0.539293103517772	-0.549402569041802
-	0.15	-	-0.532724480696440	-0.547195969996109
-	0.20	-	-0.525599266428785	-0.544023494098381
-	0.1	0.5	-0.566573347146429	-0.573550302799396
-	-	0.9	-0.592316084056838	-0.597254934810597
-	-	1.3	-0.616824333259263	-0.620393546161005
-	-	1.7	-0.640300128989056	-0.642924646973380
-	-	2.1	-0.662887590544083	-0.664846292210022

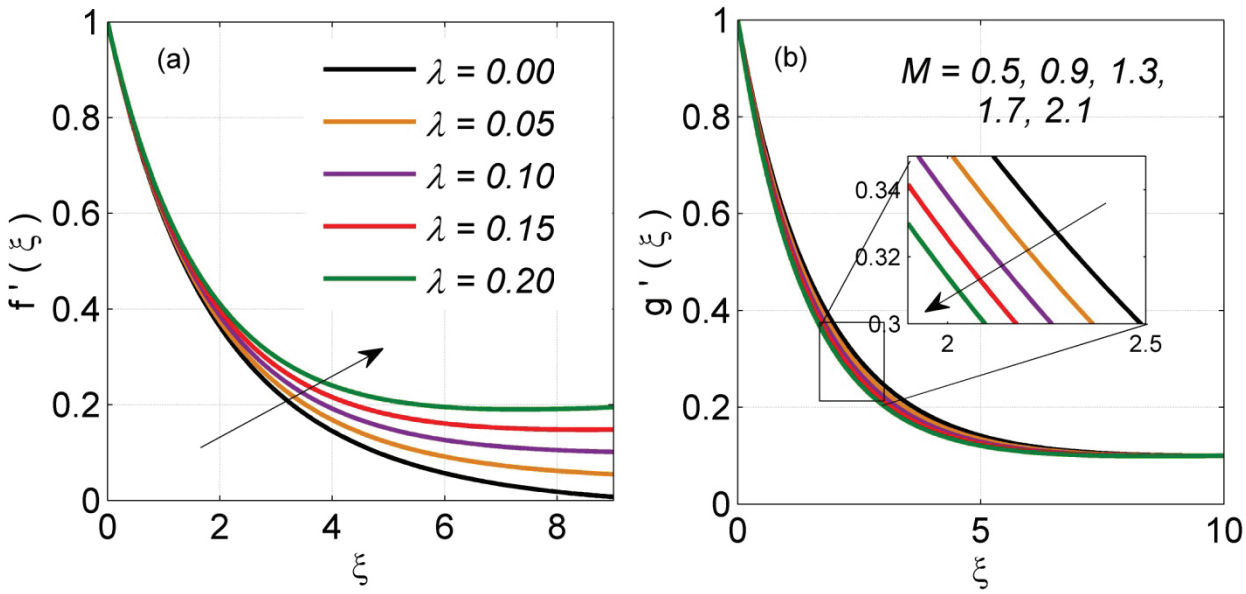

Figure 3. Velocity profile against λ, M.

Table 3. Values of $-\theta'(0)$ for variables *Nb, Nt, e* and *Pr*

Nb	*Nt*	*e*	*Pr*	$-\theta'(0)$
1	0.5	0.1	0.72	0.088935846188825
5	-	-	-	0.087689645200784
9	-	-	-	0.086290382215691
13	-	-	-	0.084722382875204
17	-	-	-	0.082970951089200
2.5	1	-	-	0.088263072055312
-	3	-	-	0.087291230091845
-	5	-	-	0.086160492596108
-	7	-	-	0.084825281499581
-	9	-	-	0.083220805678154
-	0.5	0.15	-	0.125323233938653
-	-	0.30	-	0.213938778649330
-	-	0.45	-	0.278971599721698
-	-	0.60	-	0.328321624044482
-	-	0.75	-	0.366860190093477
-	-	0.1	1	0.090073126440914
-	-	-	3	0.093790601291628
-	-	-	5	0.094902677115855
-	-	-	7	0.095477156864460
-	-	-	9	0.095835585892919

Table 4. Values of $-\phi'(0)$ for variables *Nt, h, Cr* and *Pr*

Nt	h	Cr	Pr	$-\phi'(0)$
1	0.1	0.5	0.72	0.092968930993385
3	-	-	-	0.091746864722425
5	-	-	-	0.090904931798530
7	-	-	-	0.090499811782124
9	-	-	-	0.090599171697715
0.5	0.1	-	-	0.093328137143792
-	0.2	-	-	0.175676735655186
-	0.3	-	-	0.248882170042047
-	0.4	-	-	0.314391891178914
-	0.5	-	-	0.373362399233673
-	0.1	0.0	-	0.091974413822926
-	-	0.5	-	0.093328137143792
-	-	1.0	-	0.094189985623066
-	-	1.5	-	0.094794451928946
-	-	2.0	-	0.095246246753709
-	-	0.5	1	0.094333572769597
-	-	-	3	0.096737750903311
-	-	-	5	0.097484306521909
-	-	-	7	0.097882997384870
-	-	-	9	0.098140648707370

thermophoresis boundary *Nt* that decrease of conduction of nanoparticles. Thus, temperature ascends for higher thermophoresis boundary *Nt* as illustrated in Figure 4(b). Figure 4(c) describes the variation in temperature profile as a function of *e*; ($0.15 \le e \le 0.75$) and it can be seen that temperature and convective heating increase as *e* increases. Additionally, plots diverge for around 0.0 to 3.0 and convergent with $\xi \to \infty$. Additionally, when *e* changes between

0.3 and 0.7, the Nusselt number increases in the range of 0.125323233938653 to 0.366860190093477. Further, *Pr* is the "dimensionless" amount which is the proportion of energy diffusivity to the warm diffusivity. Assuming that the liquid is taken to be moderately more thick then the worth of *Pr* increments and there is less convection in heat move rate. As the worth of *Pr* expands it will decrease the warm diffusivity. This low warm diffusivity declines temperature field as shown via Figure 4(d).

Influence of concentration distribution $\phi(\xi)$ against fluid parameters *Nt, h, Cr, Pr* has been displayed via Figure 5(a)-5(d) in a serial manner. Figure 4(a) shows the influence of concentration distribution $\phi(\xi)$ against thermophoresis *Nt* within the range $1 \leq Nt \leq 9$. This diagram demonstrates how the nanoparticle volume fraction increases with increasing thermophoresis *Nt*. Fundamentally, when a molecule applies thermophoresis to another molecule, the result is the development of particle movement from a hotter to a cooler region, which shows strengthening of the nanoparticle volume fraction as observed in Figure 5(a). Additionally, nanoparticle concentration is directly influenced by concentration Biot number. Figure 5(b) shows how the concentration profile against *h* has changed over time. When *h* changes from 0.1 to 0.5, enhancement in *h* increases concentration profile and decreases Sherwood number from 0.093328137143792 to 0.373362399233673. Figure 5(c) illustrates the variation in nanoparticle concentration in relation to *Cr* (a chemical reaction parameter). This graph demonstrates how concentration distributions gradually decrease as *Cr* increases ($0.0 \leq Cr \leq 2.0$) and become stable distant from the surface to satisfy boundary conditions. Additionally, when *Cr* increases from 0.0 to 2.0, a stronger chemical reaction cause a Sherwood number augmented in the range of 0.091974413822926 to 0.095246246753709.

Variation in concentration against *Pr* ($1.0 \leq Pr \leq 9.0$). As shown in Figure 5(d), concentration distribution decreases as *Pr* increases. Figure 6(a) manipulates effect of skin

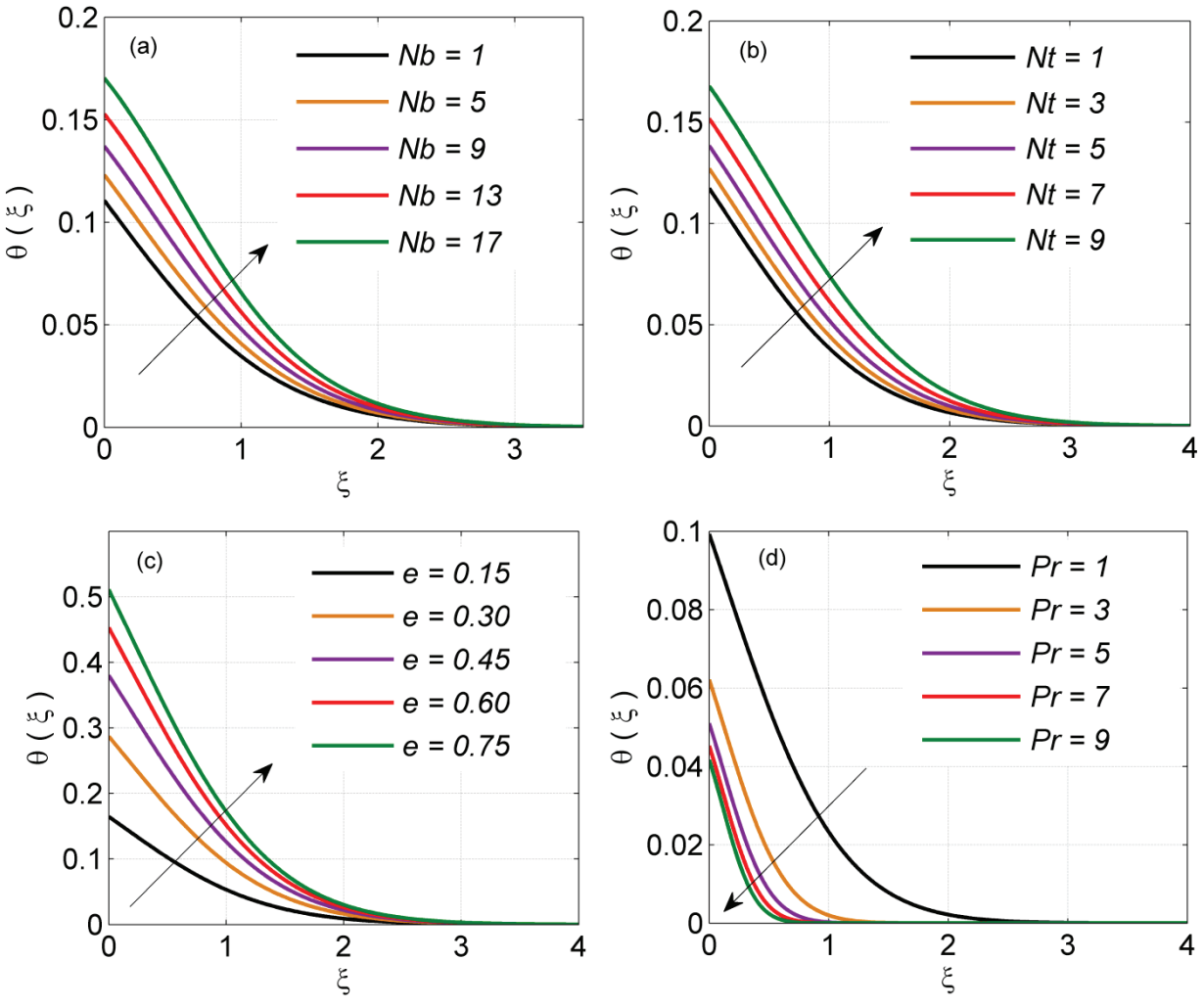

Figure 4. Temperature distribution against *Nb, Nt, e, Pr.*

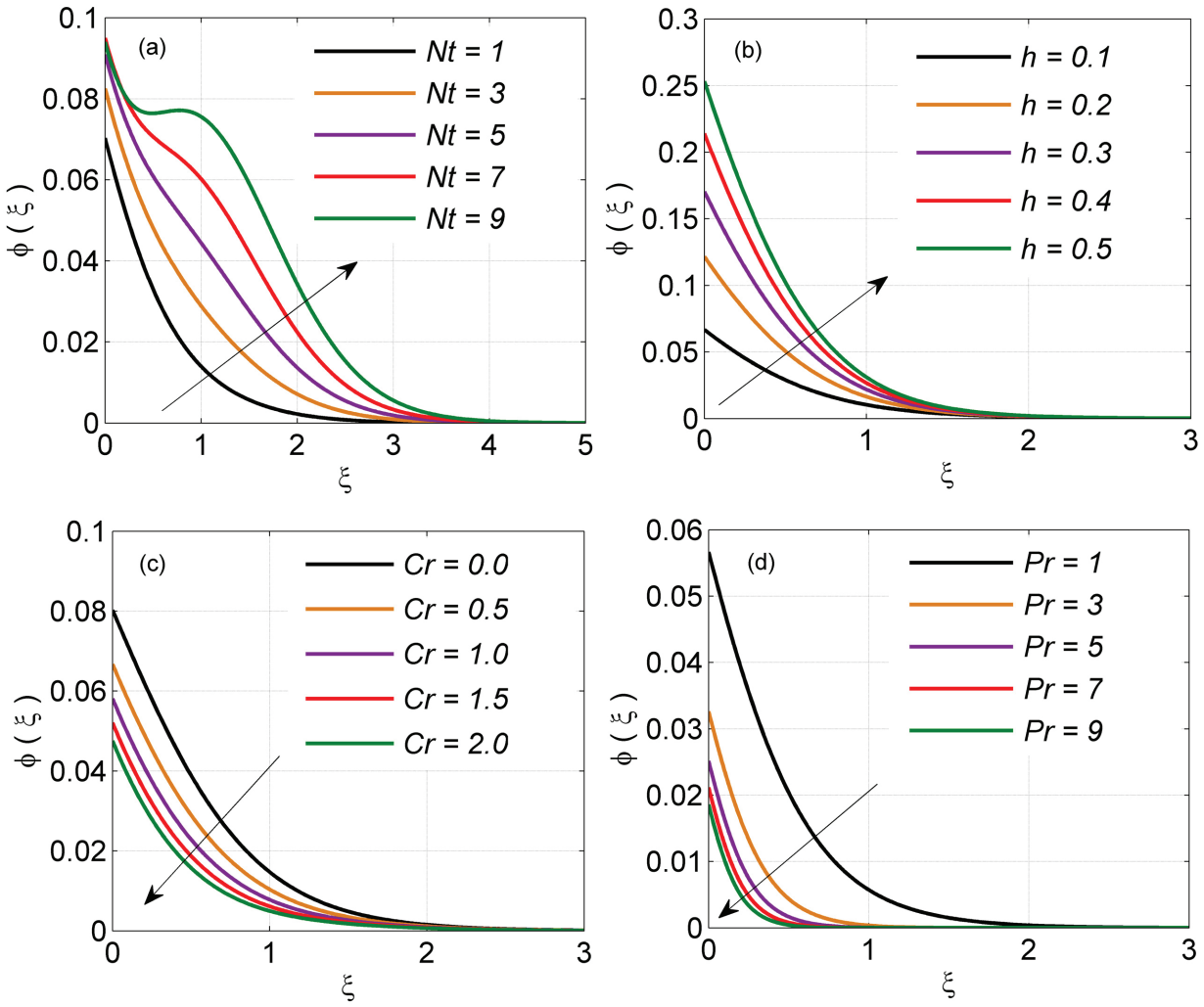

Figure 5. Concentration distribution against *Nt, h, Cr, Pr*.

friction coefficient against *Pr* in the range 1.0 to 5.0 for different β (0.08, 0.09, 0.10, 0.11, 0.12) and it is found that skin friction declines with inclination in *Pr* while augmented for higher β. Figure 6(b) shows graph of Nusselt number against *Pr* ($1 \le Pr \le 5$) for different thermal Biot number *e* ($0.1 \le e \le 0.5$) and this plot shows that Nusselt number enhances for greater *Pr* and *e*. Influence of Sherwood number against fluid parameter *Pr* for different concentration Biot number *h* ($0.1 \le h \le 0.5$) has been displayed via Figure 6(c). Sherwood number augmented with augmentation in both *Pr* and *h* as illustrated in Figure 6(c). Figure 6(d) illustrates impact of Sherwood number against Brownian motion *Nb* ($1.0 \le Nb \le 3.0$) for different Concentration Biot number *h* ($0.1 \le h \le 0.5$). Sherwood number increases very slowly and thus very minor effect of Sherwood number is noticed out for *Pr* and simultaneously it is found that higher *h* helps to increase in Sherwood number as illustrated in Figure 6(d).

Figure 7(a)-7(d) shows influence of skin friction coefficient against *Le* & *Cr*, *Pr* & *Le* , *Nb* & *Nt* and *Pr* & *Nt* respectively. Figure 7(a) manifests skin friction coefficient under the influence of Lewis number *Le* ($1 \le Le \le 3$) & chemical reaction *Cr* ($1 \le Le \le 2$) and this contour plot shows that skin friction coefficient declines with rise in values of *Le* ($1 \le Le \le 3$) and *Pr* ($1 \le Pr \le 4$). Influence of skin friction against *Pr* & *Le* has been illustrated in Figure 7(b) via contour plot. In this plot, *Pr* plays a significant role to falls down skin friction coefficient in comparison to Lewis number. Figure 7(c) manifests impact of skin friction across *Nb* ($1 \le Nb \le 3$) & *Nt* ($1 \le Nt \le 2$) and this contour shows that skin friction coefficient falls down with rise in both nanofluid parameters *Nb* & *Nt*. Moreover, combined impact of *Pr* ($1 \le Pr \le 4$) & *Nt* ($1 \le Nt \le 3$) over skin friction coefficient has been displayed via Figure 7(d). It is noticed that skin friction coefficient declines due to more dominancy of nanofluid parameter *Nt* in comparison to Prandtl number *Pr*.

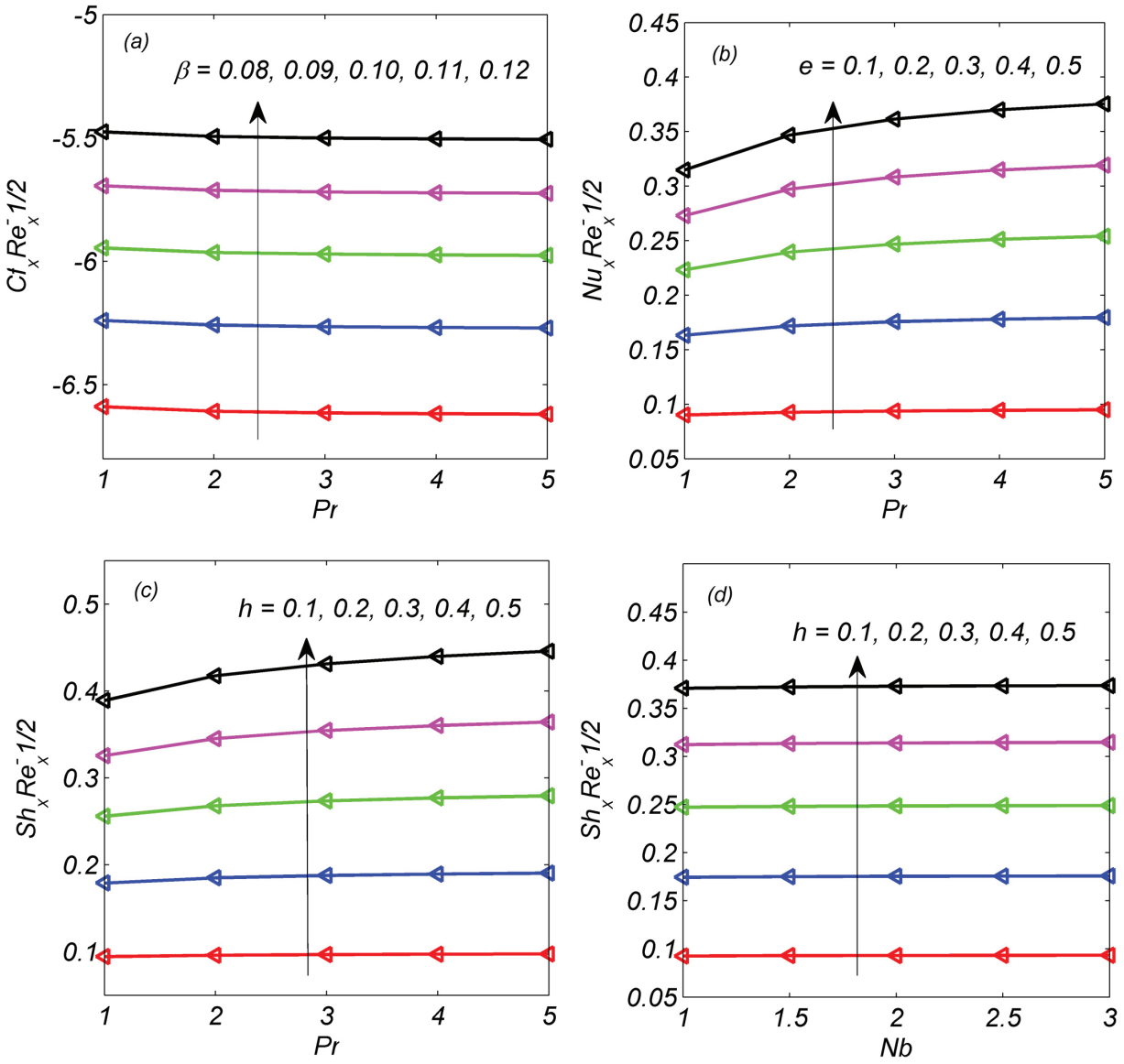

Figure 6. (a) Skin friction coefficient against β (0.08 ≤ β ≤ 0.12) & Pr (1.0 ≤ Pr ≤ 5.0), (b) Nusselt number against e (0.1 ≤ e ≤ 0.5) & Pr (1.0 ≤ Pr ≤ 5.0), (c) Sherwood number against h (0.1 ≤ e ≤ 0.5) & Pr (1.0 ≤ Pr ≤ 5.0) and (d) Sherwood number against h (0.1 ≤ h ≤ 0.5) & Nb (1.0 ≤ Nb ≤ 3.0).

CONCLUSION

Current investigation deals with the study of 3D magnetohydrodynamic flow with buoyancy forces induced by stretching surface. Major outcomes of the study are:

- Augmentation in concentration is for larger thermophoresis parameter *Nt*.
- Velocity lessens down for larger β and magnetic parameter *M* due to produced Lorentz drag force that ultimately enhances the quality of final product.
- Temperature and concentration rises with rise in thermal and concentration Biot numbers serially.
- Larger Prandtl number *Pr* declines temperature and concentration distribution.
- Skin friction coefficient declines with rise in values of *Le* and *Pr* and falls down with rise in both the values of nanofluid parameters *Nb* &*Nt*.
- Comparative study has been performed under [40, 41] to get higher accuracy and validation of the current research.

Results of the current survey have important implications for the regulation of transport phenomena and fluid velocity in a wide variety of formulation processes, which in turn benefits production, implements of technology, and

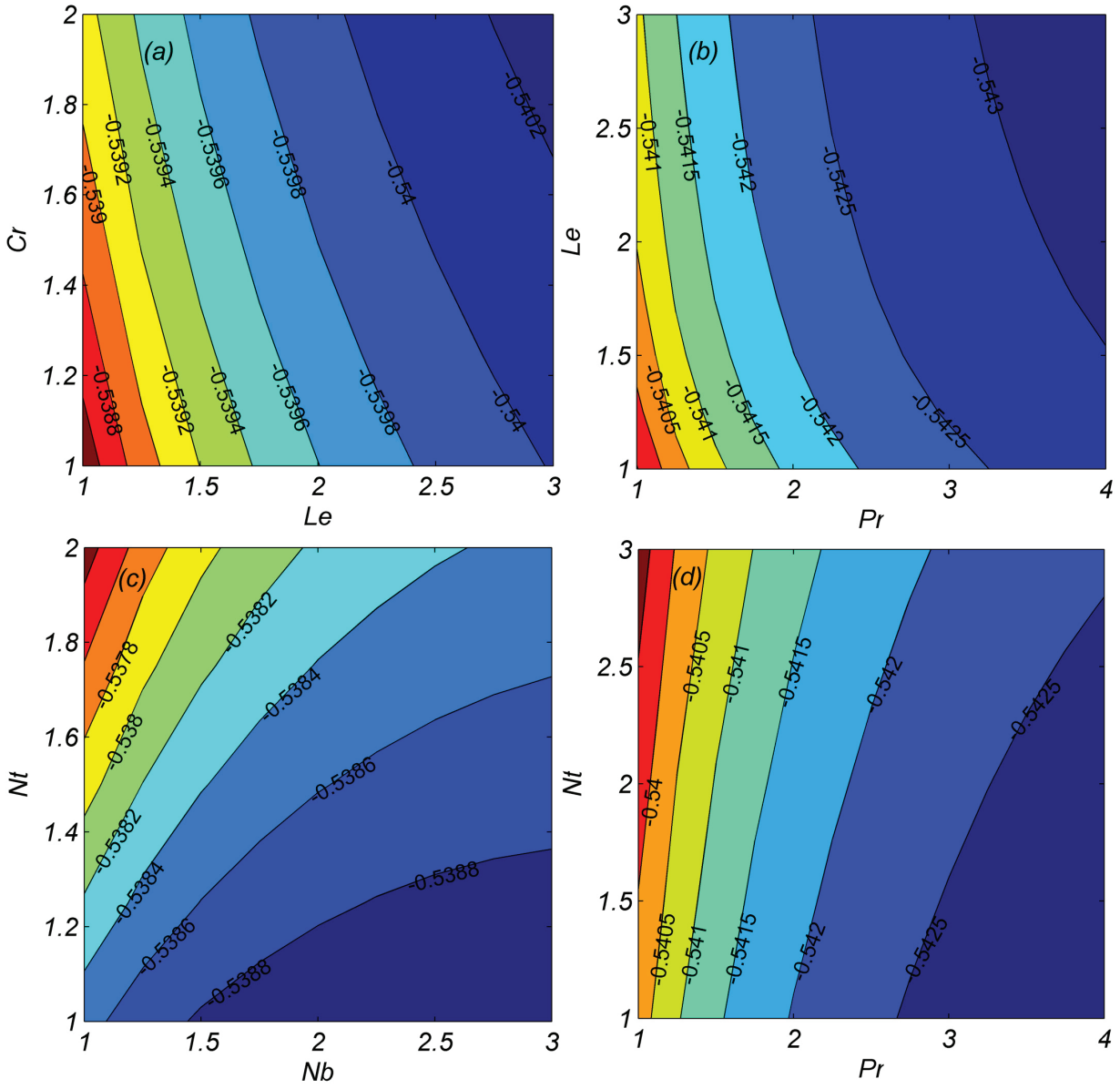

Figure 7. Skin friction coefficient for (a) Lewis number *Le* & Chemical reaction *Cr*, (b) Prandtl number *Pr* & Lewis number *Le*, (c) Brownian motion *Nb* & Thermophoresis parameter *Nt* and (d) Prandtl number *Pr* & Thermophoresis parameter *Nt*.

biological networks in their pursuit of the ideal product standard.

NOMENCLATURE

x, y, z	Cartesian coordinates
β	Casson fluid parameter
h	Concentration Biot number
λ	Free stream velocity parameter
Nt	Thermophoresis parameter
Cr	Chemical reaction parameter
M	Magnetic parameter
e	Thermal Biot number
L_1	Thermal buoyancy parameter
θ	Temperature profile
g	Gravitational acceleration
Cf_x	Skin friction coefficient along x-axis
L_2	Solutal buoyancy parameter
Pr	Prandtl number
f	Horizontal velocity profile
ϕ	Concentration profile
Cf_y	Skin friction coefficient along y-axis
Sh_x	Sherwood number
τ_{xz}	Wall shear along x- direction
Nu_x	Nusselt number
h_s	Convective mass transfer coefficient

T	Temperature
τ_{yz}	Wall shear along y- direction
C_∞	Ambient concentration
T_w	Wall temperature
T_∞	Ambient temperature
C_w	Wall concentration
ρ	density
U_w, V_w	Stretching velocity in x- and y- direction
u, v, w	Velocity components
h_f	Convective heat transfer coefficient
C	Concentration
a	Constant
L	Characteristic Length
U_0, V_0	Constant
ν	Kinematic viscosity
ξ	Similarity variable
k	Thermal conductivity
D_T	Thermophoretic diffusion coefficient
$(\rho C_p)_{nf}$	Specific heat capacity of nanofluid
Nb	Brownian motion parameter
D_B	Brownian diffusion coefficient
$(\rho C_p)_p$	Specific heat capacity of particle
σ	Electrical conductivity
B_0	Magnetic field intensity
β_C	Volumetric coefficient of solutal expansion
'	Prime denotes derivative w.r.t. ξ
U_∞	Stream velocity
β_T	Volumetric coefficient of thermal expansion
Le	Lewis number

Abbreviations

B.C's	Boundary Conditions
D.E's	Differential Equations
O.D.E's	Ordinary Differential Equations
P.D.E's	Partial Differential Equations
MHD	Magnetohydrodynamics
ANN	Artificial Neural Network
3D	Three Dimensional

AUTHORSHIP CONTRIBUTIONS

Authors equally contributed to this work.

DATA AVAILABILITY STATEMENT

The authors confirm that the data that supports the findings of this study are available within the article. Raw data that support the finding of this study are available from the corresponding author, upon reasonable request.

CONFLICT OF INTEREST

The author declared no potential conflicts of interest with respect to the research, authorship, and/or publication of this article.

ETHICS

There are no ethical issues with the publication of this manuscript.

REFERENCES

[1] Crane LJ. Flow past a stretching plate. J Appl Math Phys 1970;21:645-647. [CrossRef]

[2] Sarma MS, Rao BN. Heat transfer in a viscoelastic fluid over a stretching sheet. J Appl Math Phys 1998;222:268-275. [CrossRef]

[3] Manjunatha PT, Gireesha BJ, Prasannakumara BC. Effect of radiation on flow and heat transfer of MHD dusty fluid over a stretching cylinder embedded in a porous medium in presence of heat source. Int J Appl Comput Math 2017;3:293-310. [CrossRef]

[4] Fourier JBJ. Theorie Analytique de la Chaleur, Paris. Paris: Academie des Sciences; 1822.

[5] Cattaneo C. Sulla conduzione del calore. Atti Sem Mat Fis Univ Modena 1948;3:83-101.

[6] Bishnoi D. Pressure exertion and heat dissipation analysis on uncoated and ceramic (Al_2O_3, TiO_2 and ZrO_2) coated braking pads. Mater Today Proc 2023;74:774-787. [CrossRef]

[7] Kumar SK, Muniamuthu S, Mohan A, Amirthalingam P, Anbu Muthuraja M. Effect of charging and discharging process of PCM with paraffin and Al_2O_3 additive subjected to three point temperature locations. J Ecol Engineer 2022;23:34-42. [CrossRef]

[8] Kumar KS, Raju DBN, Arulmani J, Amirthalingam P. Design and structural analysis of liquified cryogenic tank under seismic and operating loading. Int J Mech Engineer Technol 2016;7:345-366.

[9] Muniamuthu S, Raju NL, Sathishkumar S, Kumar KS. Investigation on mechanical properties of Al 7075-Al_2O_3 metal matrix composite. Int J Mech Engineer Technol 2016;7:474-482.

[10] Choi SU, Eastman JA. Enhancing thermal conductivity of fluids with nanoparticles. In: Proceedings of the International Mechanical Engineering Congress & Exposition, ASME; 12-17 Nov 1995; San Francisco, CA.

[11] Xuan Y, Li Q. Heat transfer enhancement of nanofluids. Int J Heat Fluid Flow 2000;21:58-64. [CrossRef]

[12] Buongiorno J. Convective transport in nanofluids. J Heat Transf 2006;128:240-250. [CrossRef]

[13] Shahid A, Bhatti MM, Ellahi R, Mekheimer KS. Numerical experiment to examine activation energy and bi-convection Carreau nanofluid flow on an upper paraboloid porous surface: Application in solar energy. Sustain Energy Technol Assess 2022;52:102029. [CrossRef]

[14] Din ISU, Siddique I, Ali R, Jarad F, Abdal S, Hussain S. On heat and flow characteristics of Carreau nanofluid and tangent hyperbolic nanofluid across a wedge with slip effects and bioconvection. Case Stud Ther Engineer 2022;39:102390. [CrossRef]

[15] Ahmad M, Muhammad T, Ahmad I, Aly S. Time-dependent 3D flow of viscoelastic nanofluid over an unsteady stretching surface. Phys A Stat Mech Appl 2020;551:124004. [CrossRef]

[16] Acharya N. On the flow patterns and thermal behaviour of hybrid nanofluid flow inside a microchannel in presence of radiative solar energy. J Therm Anal Calorim 2020;141:1425-1442. [CrossRef]

[17] Rana P, Bhardwaj A, Makkar V, Pop I, Gupta G. Critical points and stability analysis in MHD radiative non-Newtonian nanoliquid transport phenomena with artificial neural network prediction. Math Method Appl Sci 2023;46:11726-11746. [CrossRef]

[18] Lu D, Ramzan M, Mohammad M, Howari F, Chung JD. A thin film flow of nanofluid comprising carbon nanotubes influenced by Cattaneo-Christov heat flux and entropy generation. Coatings 2019;9:296. [CrossRef]

[19] Alamri SZ, Khan AA, Azeez M, Ellahi, R. Effects of mass transfer on MHD second grade fluid towards stretching cylinder: A novel perspective of Cattaneo-Christov heat flux model. Phys Lett A 2019;383:276-281. [CrossRef]

[20] Rana P, Shukla N, Bég OA, Bhardwaj A. Lie group analysis of nanofluid slip flow with Stefan blowing effect via modified Buongiorno's Model: Entropy generation analysis. Differ Equ Dyn Syst 2021;29:193-210. [CrossRef]

[21] Rana P, Sharma PK, Kumar S, Makkar V, Mahanthesh B. Multiple solutions and stability analysis in MHD non-Newtonian nanofluid slip flow with convective and passive boundary condition: Heat transfer optimization using RSM-CCD. J Appl Math Mech 2023;104:e202200145. [CrossRef]

[22] Anwar MI, Shafie S, Hayat T, Shehzad SA, Salleh MZ. Numerical study for MHD stagnation-point flow of a micropolar nanofluid towards a stretching sheet. J Braz Soc Mech Sci Engineer 2017;39:89-100. [CrossRef]

[23] Shawky HM, Eldabe NTM, Kamel KA, Abd-Aziz EA. MHD flow with heat and mass transfer of Williamson nanofluid over stretching sheet through porous medium. Microsyst Technol 2019;25:1155-1169. [CrossRef]

[24] Vajravelu K, Cannon J. Fluid flow over a nonlinearly stretching sheet. Appl Math Comput 2006;181:609-618. [CrossRef]

[25] Matin MH, Nobari MRH, Jahangiri P. Entropy analysis in mixed convection MHD flow of nanofluid over a non-linear stretching sheet. J Ther Sci Technol 2012;7:104-119. [CrossRef]

[26] Jain S, Choudhary R. Soret and dufour effects on thermophoretic MHD flow and heat transfer over a non-linear stretching sheet with chemical reaction. Int J Appl Comput Math 2018;4:50. [CrossRef]

[27] Siddheshwar PG, Mahabaleshwar US. Flow and heat transfer to a newtonian fluid over non-linear extrusion stretching sheet. Int J Appl Comput Math 2018;4:35. [CrossRef]

[28] Rana P, Makkar V, Gupta G. Finite element study of bio-convective Stefan blowing Ag-MgO/water hybrid nanofluid induced by stretching cylinder utilizing non-Fourier and non-Fick's laws. Nanomaterials 2021;11:1735. [CrossRef]

[29] Kandasamy R, Muhaimin I, Ram NS, Prabhu KKS. Thermal stratification effects on hiemenz flow of nanofluid over a porous wedge sheet in the presence of suction/injection due to solar energy: Lie group transformation. Transp Porous Media 2012;94:399-416. [CrossRef]

[30] Rana P. MHD convective heat transfer in the annulus between concentric cylinders utilizing nanoparticles and non-uniform heating. AIP Conf Proc 2020;2214:020013. [CrossRef]

[31] Magagula VV, Shaw S, Kairi RR. Double dispersed bioconvective Casson nanofluid fluid flow over a nonlinear convective stretching sheet in suspension of gyrotactic microorganism. Heat Transf 2020;49:2449-2471. [CrossRef]

[32] Hosseinzadeh K, Roghani S, Mogharrebi A, Asadi A, Waqas M, Ganji D. Investigation of cross-fluid flow containing motile gyrotactic microorganisms and nanoparticles over a three-dimensional cylinder. Alex Engineer J 2020;59:3297-3307. [CrossRef]

[33] Mebarek-Oudina F, Dharmaiah G, Balamurugan KS, Ismail AI, Saxena H. The role of quadratic-linearly radiating heat source with Carreau nanofluid and exponential space-dependent past a cone and a wedge: A medical engineering application and renewable energy. J Comput Biophys Chem 2023;22:997-1011. [CrossRef]

[34] Rana P. Heat transfer optimization and rheological features of Buongiorno nanofluid in a convectively heated inclined annulus with nonlinear thermal radiation. Propuls Power Res 2023;12:539-555. [CrossRef]

[35] Bahrami HR, Ghaedi M, Attarzadeh A. Employing nonuniform magnetic fields to improve energy transfer of flow after a sudden expansion inside a miniature channel: A hydrothermal study. Engineer Rep 2024;e12847. [CrossRef]

[36] Mebarek-Oudina F, Chabani I, Vaidya H, Ismail AAI. Hybrid-nanofluid magneto-convective flow and porous media contribution to entropy generation. Int J Numer Method Heat Fluid Flow 2024;34:809-836. [CrossRef]

[37] Chamkha J, Rashad A Unsteady heat and mass transfer by mhd mixed convection flow from a rotating vertical cone with chemical reaction and Soret and Dufour effects. Can J Chem Engineer 2014;92:758-767. [CrossRef]

[38] RamReddy CH, Murthy PVSN, Chamkha AJ, Rashad AM. Soret effect on mixed convection flow in a nanofluid under convective boundary condition. Int J Heat Mass Transf 2013;64:384-392. [CrossRef]

[39] Hayat T, Muhammad T, Shehzad SA, Alsaedi A. Soret and dufour effects in three dimensional flow over an exponentially stretching surface with porous medium, chemical reaction and heat source/sink. Int J Numer Method Heat Fluid Flow 2015;25:762-781. [CrossRef]

[40] Abolbashari MH, Freidoonimehr N, Nazari F, Rashidi MM. Analytical modeling of entropy generation for Casson nano-fluid flow induced by a stretching surface. Adv Powder Technol 2015;26:542-552. [CrossRef]

[41] Khan W, Pop I. Boundary-layer flow of a nanofluid past a stretching sheet. Int J Heat Mass Transf 2010;53:2477-2483. [CrossRef]